



Article

Modular and Scalable Powertrain for Multipurpose Light Electric Vehicles

Mehrnaz Farzam Far^{1,*}, Damijan Miljavec², Roman Manko², Jenni Pippuri-Mäkeläinen¹, Mikaela Ranta¹, Janne Keränen¹, Jutta Kinder³ and Mario Vukotić²

¹ VTT Technical Research Centre of Finland, P.O. Box 1000, FI-02044 Espoo, Finland; jenni.pippuri-makelainen@vtt.fi (J.P.-M.); mikaela.ranta@vtt.fi (M.R.)

² Faculty of Electrical Engineering, University of Ljubljana, Trzaska 25, 1000 Ljubljana, Slovenia; damijan.miljavec@fe.uni-lj.si (D.M.); roman.manko@fe.uni-lj.si (R.M.); mario.vukotic@fe.uni-lj.si (M.V.)

³ THIEN eDrives, GmbH, Millennium Park 11, 6890 Lustenau, Austria; jutta.kinder@thien-edrives.com

* Correspondence: mehnaz.farzamfar@vtt.fi

Abstract: Light electric vehicles are best suited for city and suburban settings, where top speed and long-distance travel are not the primary concerns. The literature concerning light electric vehicle powertrain design often overlooks the influence of the associated driving missions. Typically, the powertrain is initially parameterized, established, and then evaluated with an ex-post-performance assessment using driving cycles. Nevertheless, to optimize the size and performance of a vehicle according to its intended mission, it is essential to consider the driving cycles right from the outset, in the powertrain design. This paper presents the design of an electric powertrain for multipurpose light electric vehicles, focusing on the motor, battery, and charging requirements. The powertrain design optimization is realized from the first stages by considering the vehicle's driving missions and operational patterns for multipurpose usage (transporting people or goods) in European urban environments. The proposed powertrain is modular and scalable in terms of the energy capacity of the battery as well as in the electric motor shaft power and torque. Having such a possibility gives one the flexibility to use the powertrain in different combinations for different vehicle categories, from L7 quadricycles to light M1 vehicles.

Keywords: charging; driving cycles; electric powertrain design; induction motor; light electric vehicle



Citation: Farzam Far, M.; Miljavec, D.; Manko, R.; Pippuri-Mäkeläinen, J.; Ranta, M.; Keränen, J.; Kinder, J.; Vukotić, M. Modular and Scalable Powertrain for Multipurpose Light Electric Vehicles. *World Electr. Veh. J.* **2023**, *14*, 309. <https://doi.org/10.3390/wevj14110309>

Academic Editors: Joeri Van Mierlo and Genevieve Cullen

Received: 9 October 2023

Revised: 1 November 2023

Accepted: 3 November 2023

Published: 11 November 2023



Copyright: © 2023 by the authors. Licensee MDPI, Basel, Switzerland. This article is an open access article distributed under the terms and conditions of the Creative Commons Attribution (CC BY) license (<https://creativecommons.org/licenses/by/4.0/>).

1. Introduction

Transportation is one of the fastest-growing sources of greenhouse gas emissions, accounting for 78% of the rise in emissions from 1990 to 2019 [1]. In 2020, transportation emissions declined by 14% solely due to the COVID-19 pandemic but witnessed a swift 12% increase in 2021 [2] following the relaxation of lockdown measures. Meanwhile, the European Union and governments worldwide have implemented various regulations and measures aimed at reducing transportation emissions on a global scale [3–7]. For instance, on 19 April 2023, the European Union and the Council modified Regulation (EU) 2019/631 to Regulation (EU) 2023/851 to enhance the CO₂ emission performance criteria for new passenger cars and new light commercial vehicles, aligning them with the heightened climate goals of the European Union. Notably, this amendment bolsters the emission targets and establishes a goal of 100% emission reduction for both cars and vans starting in 2035 [8].

Replacing internal combustion engine (ICE) vehicles with electric vehicles (EV) is a step in the right direction towards reducing emissions and supporting climate targets; however, this action alone is not enough to solve the entire problem. Additional efforts such as integrating clean energy sources, optimizing powertrains based on vehicles' missions, promoting shared vehicle usage, battery reusing, and interoperable charging technology [9] are required.

Light electric vehicles (LEVs) are particularly suitable for urban and suburban environments, where high speed and long range are not the main priorities. LEVs have lower energy consumption and higher vehicle weight-to-payload ratios, and they require fewer resources for production compared to other EVs [10]. This makes them more efficient and affordable, especially for large-scale production and shared mobility scenarios.

Table 1 provides an overview of the specifications of some L7e-C category EVs available on the market. All the vehicles listed in this table meet the European regulations outlined in (EU) No 168/2013 [11], which specify that L7e-C vehicles must have a maximum continuous rated power of no more than 15 kW and a maximum speed of no more than 90 km/h.

Table 1. Specifications of some L7e-C category EVs available on the market.

Name	Power (kW)	Max Torque (Nm)	Max Speed (km/h)	Voltage (V)	Battery Type, Capacity (kWh)	Range (km)
Honda Micro Commuter	15	N/A	80	N/A	Li-ion, N/A	96
Mahindra e-Supro van	15	90	60	72	Li-ion, 15	115
Mahindra Treo	7.5	42	55	48	Li-ion, 7.3	141
Microlino	11	89	90	N/A	Li-NMC, 14	230
Renault Twizy	13	57	80	58	Li-ion, 6.1	100
Regis Epic0 Compact	15	N/A	75	144	Li-NMC, 15.2	140
PILOT CAR, P-1000	10	102	55	48	Li-ion, 26	220
Tazzari Zero	15	150	90	80	Li-ion, 14.2	150

The design of a powertrain starts by defining various quantities such as power, torque, speed, voltage, battery capacity, and range of the vehicle. The power and torque requirements of an electric traction motor depend on the vehicle's desired performance characteristics, size, and weight. An accurate definition of the performance characteristics and, therefore, a reduction in the vehicle's energy consumption require knowledge of the vehicle's actual driving cycles and mission. As an example, Lindh et al. [12] used an actual driving cycle of a bus route in Lappeenranta to investigate the speed and torque requirements for a heavy-duty vehicle. Based on these requirements, the authors proposed a permanent magnet traction motor design suitable for hybrid buses. However, the literature on LEV powertrain design rarely considers the associated driving missions. Instead, the powertrain is first parametrized and settled, and then, an ex-post-performance assessment is conducted using various driving cycles [13–16].

Different battery technologies for EVs are reviewed and compared in [17]. Lithium-ion (Li-ion) batteries are the most frequently utilized battery type in EVs due to their significantly higher energy density (Wh/kg) compared to other alternatives. The two most used Li-ion chemistries are NMC (nickel–manganese–cobalt) and LFP (lithium–iron–phosphate). NMC cells provide a higher energy density and have a better charging performance at low temperatures, whereas LFP cells are more affordable and have a longer cycle life. The high energy density of NMC is vital for providing sufficient ranges for everyday electric driving, especially for LEVs, in which the mass and physical dimensions of the battery have strict limitations. On the other hand, the price range of LFP would better fit with LEVs. However, if an LEV is to be charged at a reasonable speed in cold-climate environments, expensive and heavy thermal management systems would be required in the case of LFP batteries. Hence, optimal cell chemistry is a compromise of price, energy density, and cold-climate performance. The battery capacity is determined based on various factors, such as the vehicle's energy consumption, the expected driving conditions, the desired driving range, the weight of the vehicle, and the efficiency of the electrical motor. Battery cost is a significant factor contributing to the price of EVs. The cost breakdown of batteries

can be classified into four primary segments: materials, labor, assembly, and overhead. Materials constitute the largest portion, representing approximately 60% of the total battery cost. Anticipated reductions in battery cell and pack costs are expected to occur gradually due to advancements in battery material chemistry, improvements in battery cell design, and a decrease in assembly expenses resulting from increased production volumes and learning. For instance, it is predicted that the global price per kWh of a battery pack will decrease by approximately 64% in 2050 compared to 2019 [9]. Nevertheless, the current high cost of batteries makes small LEVs a more cost-effective choice compared to larger EVs, given their smaller battery size.

The voltage levels of LEVs available on the market typically range from 48 to 80 V. The specific voltage level of an LEV is determined during the design stage, considering several factors such as the power and torque requirements of the motor, the desired range of the vehicle, and the weight and cost constraints of the battery pack. Using higher voltages in electric vehicles can be more cost-effective for energy distribution as lower currents require smaller cable cross-sections and connectors. In addition, higher voltage levels offer greater powertrain scalability towards higher vehicle categories with superior performance characteristics, such as increased torque, power, and vehicle speed.

In this paper, we present the design of a modular and scalable electric powertrain for L7e-C category EVs with multipurpose usages (transporting people and goods), with a focus on the motor, battery, and charging requirements. The modularity and scalability of the proposed electric powertrain allow one to modify each component according to the vehicle's mission, without affecting the overall powertrain concept. This approach facilitates the adaptation of the powertrain for use in higher classes of vehicles, such as M1. To ensure that the powertrain components are rightly sized according to the vehicle's mission, the associated driving missions and operational patterns are considered in the design from the very first stages.

This research has been presented at the EVS36 Symposium in Sacramento, USA, in June 2023.

2. Materials and Methods

2.1. Vehicle Requirements and Specifications

The first step in powertrain design involves setting the base specifications and requirements of the vehicle. As mentioned previously, this paper focuses on L7e light four-wheel EVs. To comply with European regulations, the vehicle properties and specifications were defined based on regulation (EU) No 168/2013 [11], as follows: a mass in running order of up to 600 kg (without the battery and payload), a top speed of 90 km/h, and a maximum continuous power of 15 kW. The total gross weight of the vehicle is assumed to be 1200 kg (150 kg of which is the battery and 450 kg of which is the payload). The 1-D vehicle model was described using basic parameters with the following values: wheel's radius $R_w = 0.31$ m, vehicle's front area $A_v = 2.17$ m², wind drag coefficient $C_x = 0.3$, tires' pressure $p_t = 3$ bar, mass density of air $\rho = 1.2$ kg/m³, and rolling resistance coefficient C_r , which is a function of vehicle speed and whose value varies between 0.0083 and 0.011.

Other basic properties required for the powertrain design include the vehicle's driving range and its torque and power profiles. To ensure that the powertrain components are appropriately sized according to the vehicle's mission, the associated driving missions and operational patterns should be considered from the very first stages of design. For this purpose, we used a driving cycle generated based on typical trips in a European city, Helsinki, to study the vehicle's driving range, torque-speed profile, and power requirements. This driving cycle was dynamically created using an in-house simulation tool [18] taking into account the speed limits, traffic lights, road curvature, historical traffic data, and predefined limits for acceleration and deceleration. The specific driving cycle was chosen from a large set of routes and their corresponding driving cycles to represent a typical trip in the Helsinki region, with a mix of urban and suburban driving conditions. It is worth noting that the presented driving cycle also included terrain shape in the form of

road elevation changes during the velocity profile. The speed and elevation profiles of this driving cycle are illustrated in Figure 1.

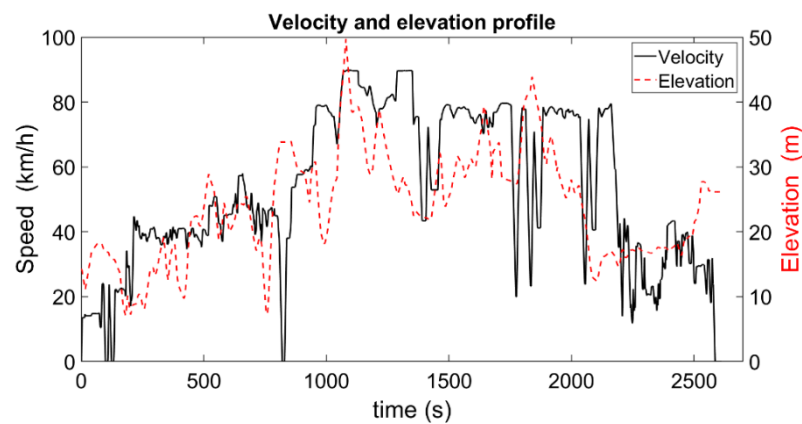


Figure 1. Simulated speed and elevation profiles of the Helsinki region with a mix of urban and suburban driving conditions.

According to the highest allowable vehicle speed (90 km/h), a wheel radius of 0.31 m (R15), and the maximum electric motor rotational speed (10,000 rpm), we defined a gear ratio of 12:1 with a mean efficiency of 95%. Applying the identified Helsinki driving cycle and incorporating the upper boundary conditions, we calculated the vehicle's needed torque and shaft power requirements. Figures 2 and 3 present the power and torque profiles of an electrical machine for the Helsinki driving cycle, without and with considering a 450 kg payload in the vehicle's weight, respectively.

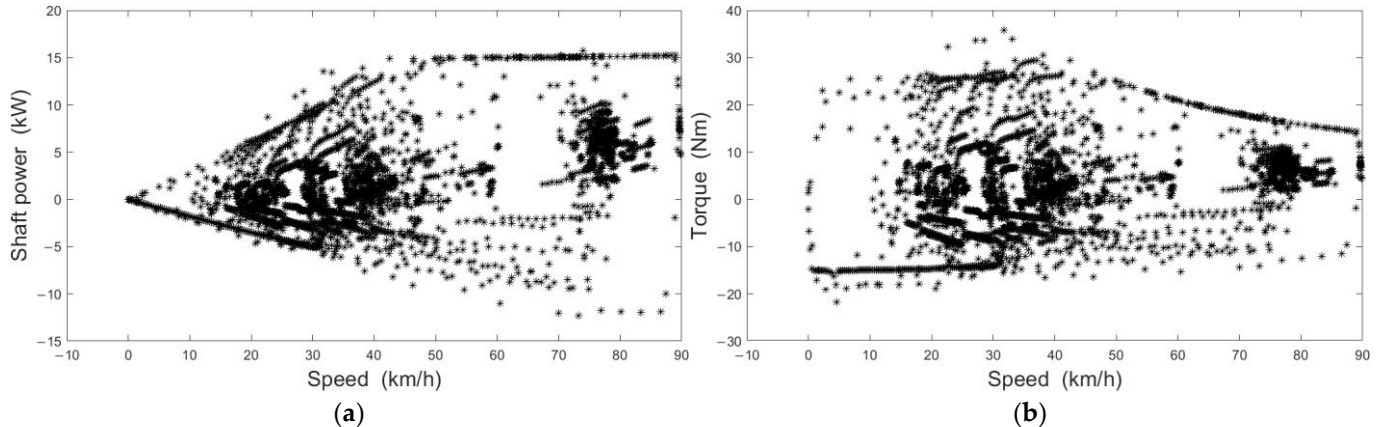


Figure 2. (a) Power–speed and (b) torque–speed profiles of an electrical machine for the Helsinki driving cycle with a total vehicle weight of 750 kg.

Further, the energy consumption at each driving point and the cumulative needed energy within one cycle were calculated. The overall energy consumed in the case of an unloaded vehicle in one driving cycle (38.2 km), including the road profile in the form of elevation (Figure 1), is 2.73 kWh. In the case of a fully loaded vehicle (with a payload of 450 kg), the consumed energy is 3.56 kWh. To achieve a range of approximately 100 km and enable shorter charging times even with standard three-phase home charging facilities, the battery must provide enough energy to allow the vehicle to complete at least three Helsinki driving cycles, covering a total distance of 114.6 km. For such a distance, the electric energy consumed by the battery ranges between 8.16 kWh and 10.68 kWh. If we assume a 30% battery safety margin, the battery should have an energy capacity in the range of 15 kWh.

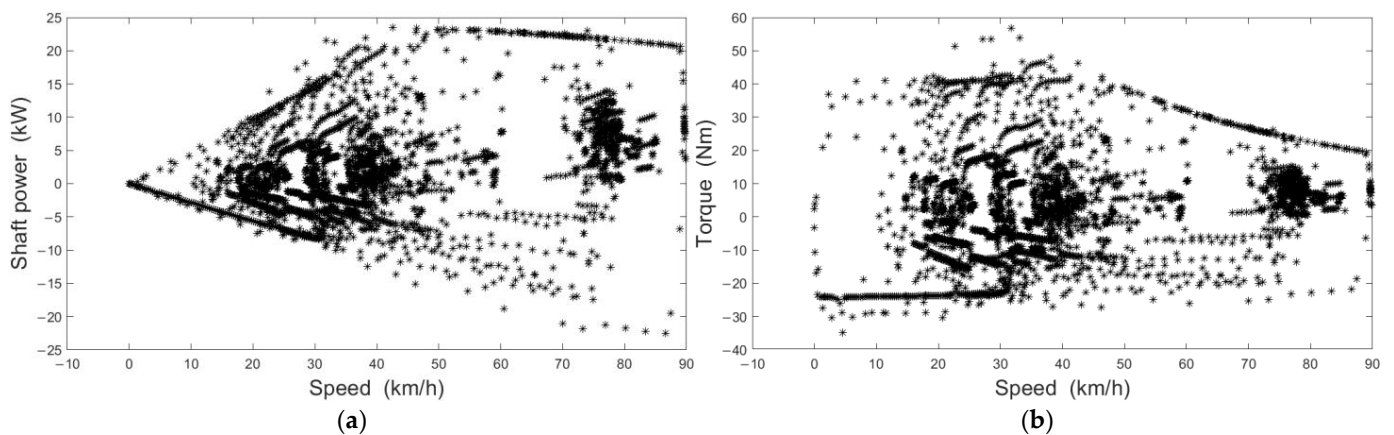


Figure 3. (a) Power–speed and (b) torque–speed profiles of an electrical machine for the Helsinki driving cycle with a total vehicle weight of 1200 kg (including a 450 kg payload).

Based on the calculated torque and power profiles (Figures 2 and 3), the following electro-mechanical requirements were established for the design of the electrical machine:

- The electrical machine should be capable of delivering a shaft power of 15 kW in the constant power operational region, with this region extending up to a speed of 90 km/h corresponding to a motor speed of 9240 rpm (Figure 2a).
- The machine should have a nominal torque of approximately 40 Nm (Figure 2b) in the case of an unloaded vehicle. Meanwhile, the maximum power and maximum torque should reach up to 23 kW and 60 Nm, respectively, due to the vehicle’s full payload (Figure 3).
- The electric machine’s torque–speed curve should have a corner point between 35 and 50 km/h, corresponding to a motor speed of around 3600–5100 rpm, to ensure that the torque demands remain within the region of highest efficiency for the electric machine.
- The variation of the torque between 40 Nm and 60 Nm should depend on the vehicle’s payload and the driving cycle’s starting condition.

2.2. Traction Motor Design

Induction motors (IMs) and permanent magnet synchronous motors (PMSMs) are the most used electric traction motors in EVs. IMs are robust, reliable, and cost-effective, and their torque characteristics are proportional to the current. PMSMs, on the other hand, have higher efficiency, power density, and torque density than IMs. PMSMs perform better at high speeds and can produce high torque at low speeds, but they are more complex and expensive to produce due to the use of critical raw materials.

The type of traction motor chosen for an EV depends on the specific requirements. PMSMs are often used for high-performance EVs, while IMs are preferred for low-cost EVs. In this work, we chose an IM for the traction motor due to its robustness and to avoid the use of rare earth materials.

The electromagnetic field of an induction machine is governed by

$$\nabla \times \left(\frac{1}{\mu} \nabla \times \mathbf{A} \right) = \mathbf{J}, \quad (1)$$

where μ is the permeability; \mathbf{A} is the magnetic vector potential; and \mathbf{J} is the current density. In a 2D analysis, \mathbf{A} and \mathbf{J} have components only in the axial direction. The right-hand side of (1) equals zero in the air gap and in the laminated iron of an electrical machine as the

current density is zero or close to zero in those areas. Considering eddy currents induced in the rotor's winding, one can present the field equation of the rotor bars as

$$\sigma \frac{dA}{dt} + \nabla \times \left(\frac{1}{\mu_0} \nabla \times A \right) = \frac{\sigma \Delta v_m}{l} e_z, \quad (2)$$

σ being the rotor bar's electrical conductivity, Δv_m being the voltage drop between the ends of the m th bar, l being the total length of the bar, and e_z being the unit vector in the axial direction.

The traction motor was simulated using the 2D transient magnetic finite element method in the Altair Flux software. The end-region elements (end-winding and end-ring resistances and leakage inductance) were analytically calculated and added as lumped elements to the external electrical circuit. The boundary conditions and requirements for designing the motor were selected for the gear ratio 12:1 as follows:

- A continuous power of 15 kW through the whole speed range (Figure 2a) and a peak power of 23 kW (Figure 3a).
- A nominal torque of 40 Nm (Figure 2b) and a maximum torque of 60 Nm (Figure 3b)
- A maximum torque of 70 Nm at zero speed to overcome the curb (calculated based on the wheel's size, the vehicle's mass, and a curb height of 15 cm).
- A nominal phase RMS voltage in the range of 125 V to 175 V, allowing lower electric currents and smaller electric power wires cross-sections.
- The maximum rotational speed of the motor should be 10,000 rpm, due to the 90 km/h maximum vehicle speed limitation, wheel size, and gearbox ratio).
- A maximum motor efficiency > 92%.

To minimize the motor's size and maximize its overload operational capabilities, we selected a liquid cooling system instead of an air-cooling system. The liquid cooling system offers a higher heat removal capability, especially when the vehicle is heavily loaded at lower rotational speeds.

Considering these conditions and requirements, we simulated and studied various IM designs. A comprehensive analysis was conducted to determine the optimal number of stator slots and rotor bars to minimize the torque pulsations at the nominal operating point [19,20]. The analysis showed that the lowest torque pulsation occurred with 36 stator slots, 50 rotor bars, and 2 pole pairs. However, using 50 rotor bars would result in a thin rotor tooth. To ensure stable manufacturing and adequate rotor strength, the design with the second-lowest torque pulsations, namely, 30 rotor bars, was chosen. This decision aligns with our cost-effectiveness objectives, as the combination of 36 stator slots and 30 rotor bars can be produced using conventional methods and readily available electrical laminations. In addition, the shape of the rotor bars was chosen to enhance the critical torque value and reduce factors such as eddy current losses, magnetizing currents, and manufacturing complexity. The lamination design and 3D form of the proposed traction motor with liquid cooling are presented in Figure 4a and Figure 4b, respectively. The winding layout, shown in Figure 4c, has a double-layer fractional slot winding with a coil span of eight slots and a winding factor of 0.945.

To reach a cost-effective scalability, the cross-sections of the stator and rotor lamination were fixed, and the axial length of the motor (with proper adjustment of the number of turns in the stator winding) was varied according to the voltage and power requirements. Different axial lengths were investigated to determine the optimized length for the motor. Table 2 presents the main parameters of three of these designs. The results of these three designs, along with the analysis of the crossroad dynamics in the form of acceleration rates, will be presented in Section 3.

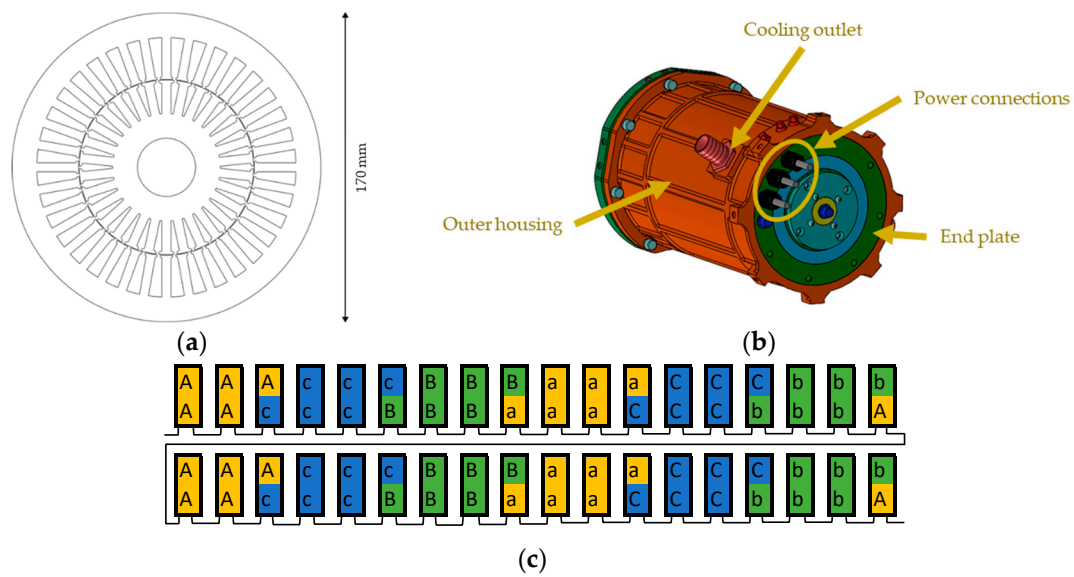


Figure 4. (a) 2D cross-section, (b) schematic 3D view, and (c) winding layout (with three phases A, B, and C, small letter denoting the opposite direction of a coil side) of the proposed traction motor.

Table 2. Design specifications of the proposed traction motors.

Motor Parameter	Motor 1	Motor 2	Motor 3
Continuous power (kW)		15	
Core material		Cogent M270-35A	
Material of stator winding and rotor bars		Copper	
Number of pole pairs		2	
Number of stator slots/rotor bars		36/30	
Stator core outer diameter (mm)		170	
Stator core inner diameter (mm)		96.8	
Air gap width (mm)		0.4	
Shaft diameter (mm)		32	
Thickness of lamination (mm)		0.35	
Rotor end ring segment resistance (Ω , 100 °C)		3.04×10^{-6}	
Rotor end ring segment inductance (H)		4.82×10^{-9}	
Core length stator/rotor (mm)	200	150	100
Number of turns per coil	5	6	8
Stator winding one-phase resistance (Ω , 100 °C)	0.054	0.0672	0.1011
Stator end winding inductance (H)	4.14×10^{-5}	5.98×10^{-5}	1.07×10^{-4}
Peak power (kW)	47.5	40.6	29.9
Base speed (rpm)	4000	4380	4680
Peak torque (Nm)	127.0	97.3	66.9
Maximum efficiency (%)	94.5	93.9	92.5
Total weight (kg)	46.1	38.3	30.8

2.3. Battery and Frequency Inverter

Based on the above-defined nominal phase RMS voltage level, the maximum allowable battery voltage could range from 340 V to 475 V. Another voltage limit was set by the off-the-shelf frequency inverter needed to drive the designed traction motor. We decided to use a SEVCON Gen4Size8 frequency inverter [21] with a maximum voltage limit of 400 V. To achieve the maximum voltage level of 400 V, we used 96 Li-ion NMC battery cells from KOKAM (model: SLPB100216216H [22]) connected in series, each having a capacity of 40 Ah. When using cells with an average voltage of 3.7 V, the battery stack delivers a maximum energy of 14 kWh. The proposed battery assembly provided sufficient energy to fulfill the defined range of the vehicle.

The battery designed for the vehicle had integrated BMS, contactors, fuses, DC/DC converter (400 V/12 V, 1.2 kW), and air-cooling fans in the battery box (Figure 5). This battery design featured an energy storage system with an energy capacity of 14 kWh, fulfilling all the requirements regarding voltage, vehicle range, overload capability, fast charging, and safety concerns (battery's structural integrity). Moreover, the battery was built modularly, so its energy capacity could be scaled up to 25 kWh, for example, for the M1 vehicle type just by substituting the battery cells with the ones that have a higher 60 Ah capacity, such as the KOKAM Model: KCL216060EN1 [23].

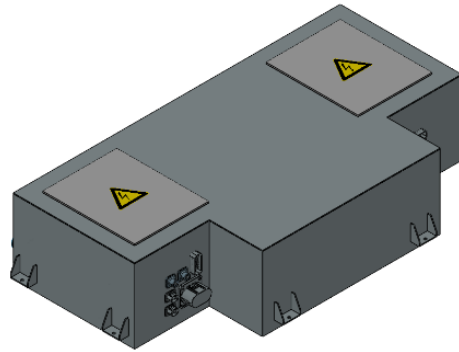


Figure 5. Modular battery for different vehicle classes (L7 to M1).

2.4. Charging Requirements

A detailed analysis of the vehicle's utilization was conducted to determine the required power of the charging system. In this work, vehicle utilization is referred to as duty cycles and encompasses the trips that a vehicle is expected to make during the day. The duty cycles are presented as schedule-format descriptions of the driven route's origins and destinations, non-driving related activities (such as cargo loading and unloading), and breaks from all activities when the vehicle is not occupied. The cycle profiles can be generated via mesoscopic simulations such as activity-based transport modeling (ABTM) [24]. We implemented the duty cycles into an in-house microscopic simulation tool [18] to study the charging requirements of the vehicle while considering the driving cycles, vehicle dynamics, and charging module. In the simulation, it was assumed that a fleet of about 28,000 vehicles with a utility rate of 50% had been distributed around the capital region of Helsinki (i.e., Helsinki, Espoo, Vantaa, and Kauniainen), providing a shared fleet for 24/7 transportation (e.g., people during the day and goods at night).

Figure 6a shows the simulated daily distance driven by each vehicle in the fleet. As shown in this Figure, the average distance exceeds 200 km, and some vehicles travel over 300 km per day. Figure 6b displays the maximum available charging time between each trip, assuming that charging is feasible at all locations where the vehicles park.

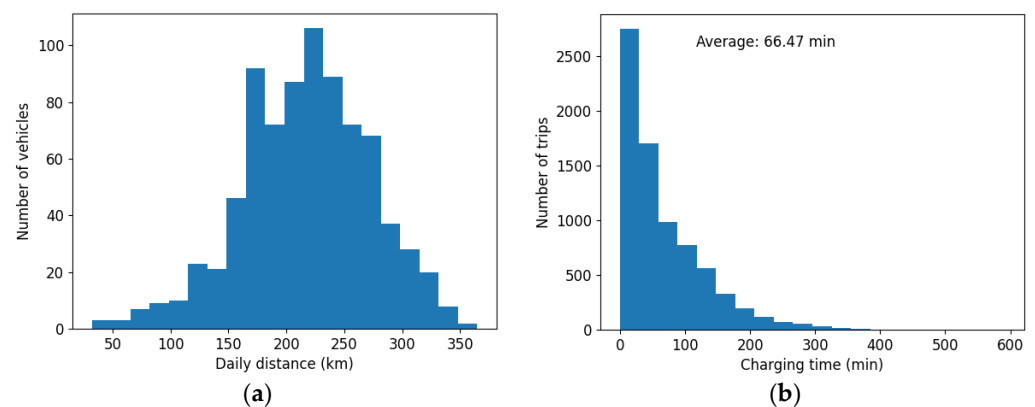


Figure 6. (a) Distribution of the simulated daily distance of each vehicle and (b) maximum available charging time between the trips.

To gain an understanding of the vehicle’s operation in a more realistic situation where charging is not always possible, the parking locations of the vehicles from the initial simulations were analyzed and the 100 most-often-used locations were set to be equipped with a charger, while the other parking locations were left without charging facilities. Out of the 100 charging locations, 20% were equipped with fast 7 kW chargers and the rest with slower 3.7 kW chargers. The results of these two charging scenarios are compared in Section 3.

3. Results and Discussion

Figure 7 presents the efficiency maps of the three motor designs, which were calculated using the 2D finite element method. The efficiency maps show the maximum achievable power values without any electric current limitations. As can be seen from the efficiency maps, Motor 1, with a corner point at 4000 rpm, has the largest efficiency area in comparison to the other motors.

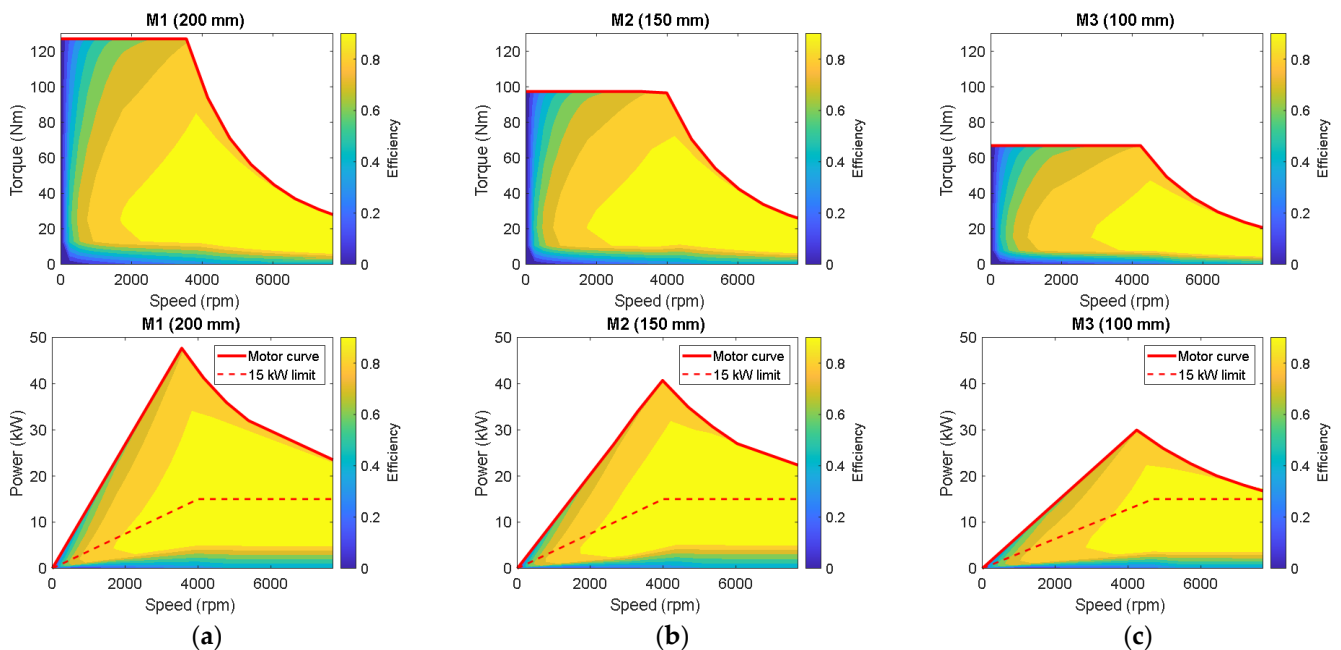


Figure 7. Efficiency maps of motor variants with different core lengths: (a) Motor 1 (200 mm); (b) Motor 2 (150 mm); and (c) Motor 3 (100 mm). The dashed lines represent the power–speed profiles respecting the 15-kW continuous power limit.

The vehicle’s dynamics were simulated with these three motor designs. In the simulation, the resistive forces acting on the vehicle (e.g., slope, friction, air drag) and the total inertia, scaled to the electrical motor, were considered. For the gearbox and differential, a constant efficiency level of 95% was assumed. The comparison of the motors was carried out on roads with slopes ranging from 0% to 26% (maximum road slope), in terms of the maximum achievable speed and acceleration times from 0 to 40 km/h. The acceleration test results are presented in Table 3. According to these results, Motor 1 achieves the highest speeds on all the slopes and outperforms the other two motors in the acceleration tests.

Table 3. Maximum achievable Speed on different slopes for a fully loaded vehicle (1200 kg).

Motor Variant	Top Speed 0% Slope	Top Speed 26% Slope	Acceleration 0% Slope	Acceleration 26% Slope
Motor 1	90 km/h	41.7 km/h	4.00 s	14.12 s
Motor 2	90 km/h	39.6 km/h	5.14 s	N/A
Motor 3	90 km/h	38.9 km/h	7.57 s	N/A

The torque's range was established by analyzing the driving cycles, as described in Section 2.1. Nevertheless, to validate the torque requirements and to make any necessary adjustments, the real-world urban driving cycle acceleration time was considered as well. This will further permit the adjustment of the torque characteristics of the traction motor and gearbox ratio, if needed, to fulfill the high dynamics of an EV in urban driving conditions.

The acceleration time in the urban driving condition was measured by conducting an acceleration test on a vehicle with an ICE that had similar size and weight characteristics to the vehicle under investigation. The acceleration test resulted in a time of approximately 4 s to reach from 0 km/h to 40 km/h. The results of this test were then utilized to define the acceleration torque requirements by inputting the data into a MATLAB R2020b software program that was designed based on the vehicle's equation of motion.

The developed MATLAB R2020b software allows for the simulation of changes in the dynamic performance of the EV powertrain, considering factors such as the torque–speed characteristic of the traction motor, the gearbox ratio, vehicle mass (1200 kg), vehicle shape (drag coefficient), wheel diameter, slope coefficient, and tire pressure. The output of the software is the calculated speed of the vehicle over time, from which the acceleration can be determined.

Figure 8 presents the power–speed and torque–speed curves, along with the transient acceleration behavior, of all three motors on the 0% slope, assuming a fully loaded vehicle with a total mass of 1200 kg. According to the results, the vehicle with Motor 1 fulfills the acceleration requirements from 0 to 40 km/h in 4 s and, therefore, is chosen as the traction motor of the proposed vehicle.

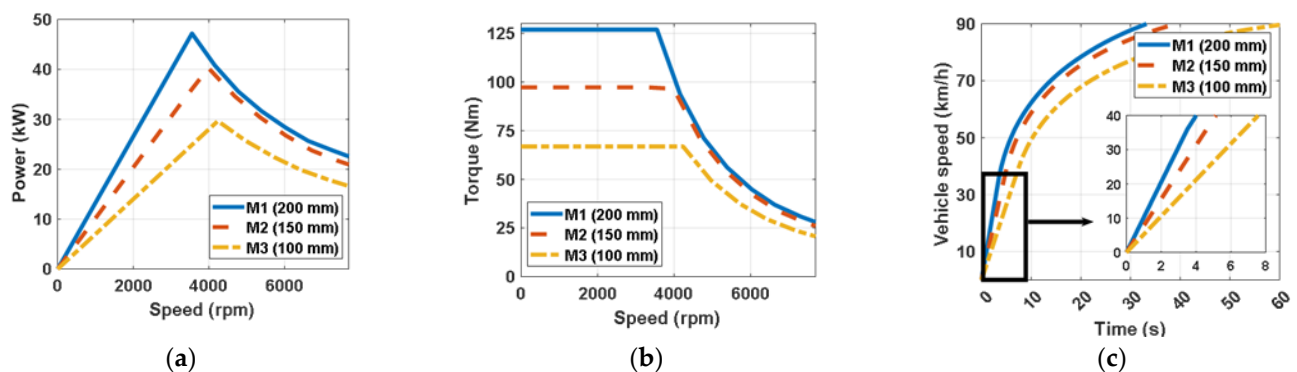


Figure 8. Influence of (a) power–speed and (b) torque–speed curves on (c) the vehicle's acceleration.

Table 4 summarizes the results of the following two charging scenarios: one with charging available at all parking locations and the other with charging available at only 100 locations. In the first scenario, all the scheduled trips were fulfilled without the battery state of charge (SOC) dropping below 35%. In the second scenario, some vehicles could not complete their trips due to the high daily distances. Nevertheless, on average, 92% of the daily target distance was covered, and the issues were mostly related to the very last trip of the day. It is worth noting that the simulations did not consider certain driver behaviors, such as selecting a vehicle with a higher SOC or choosing a parking spot with a charger instead of one without. Accounting for these factors would likely increase the likelihood of completing all the trips. Therefore, 7 kW was chosen as the maximum charging power of the vehicle. With such power, the battery could be charged from zero to 100% SOC in slightly more than 2 h.

In this paper, we highlight the importance of tailoring the powertrain of the vehicle according to its anticipated driving mission, resulting in optimized energy efficiency. While standard driving cycles can serve this purpose, they typically do not include complex and variable driving conditions such as traffic congestion, elevation changes, and weather conditions. By using real-world driving cycles, we can incorporate these variables when designing the powertrain. In cases where real-world driving cycles are not accessible, accurately simulated driving cycles, such as the one used in this paper, offer a suitable al-

ternative. To illustrate the performance and advantages of our approach, we will prototype an LEV with the proposed powertrain and test its efficiency under various driving cycles, including the standard, real-world, and simulated scenarios.

Table 4. Summary of simulated duty cycle with two charging scenarios.

Charging Scenario	Completed Daily Distance, (Mean (Min–Max))	Trips/day, (Mean (Min–Max))	Completed Distance vs. Target
Slow charging (3.7 kW) available at all parking locations	217.6 km (32.1–364.7) km	10.5 (1–20)	100%
Slow charging (3.7 kW) at 80 locations and fast charging (7 kW) at 20 locations	196.6 km (32.1–326.6) km	9.8 (1–17)	92.4%

While our research has primarily addressed the technical and operational aspects of the powertrain, it is important to acknowledge that cost considerations play a significant role in the real-world adoption of electric vehicles. Future studies should delve deeper into the economic aspects of electric vehicle development, exploring cost-effective strategies for component design, manufacturing, and charging infrastructure. This will help bridge the gap between the technical advancements presented in this paper and the practical affordability of electric vehicles, ultimately contributing to their wider adoption and sustainability.

4. Conclusions

This paper presents the design of an electric powertrain for multipurpose light electric vehicles, focusing on the motor, battery, and charging requirements. The first step of the design involved studying a driving cycle from a typical European city such as Helsinki, to derive the vehicle's driving range, torque–speed profile, and power requirements. This ensures that the proposed design is optimized according to the vehicle's driving missions and operational patterns. We explored several cross-section designs for IMs, each with varying pole pair and slot numbers, and ultimately chose the design that aligned with the driving cycle requirements. In the next step, to achieve economical scalability, we maintained consistent cross-sections of the motor while adjusting its axial length. We explored various axial lengths and selected the most optimal motor length based on the torque and power profile and the vehicle's dynamics. The most efficient motor was found to meet the vehicle dynamics' criterion of accelerating from 0 to 40 km/h in 4 s. The battery capacity was estimated based on the driving range. The maximum charging power of the vehicle was set to 7 kW after a detailed analysis of the vehicle's expected utilization throughout the day.

Author Contributions: Conceptualization, all authors; methodology, all authors; software, D.M., R.M., M.R., and M.V.; validation, D.M., R.M., M.R., and M.V.; formal analysis, D.M., R.M., M.R., and M.V.; investigation, D.M., R.M., M.R., and M.V.; resources, D.M. and J.P.-M.; data curation, D.M. and M.R.; writing—original draft preparation, M.F.F.; writing—review and editing, all authors; visualization, all authors; supervision, D.M. and J.P.-M.; project administration, J.P.-M.; funding acquisition, J.P.-M., D.M., J.K. (Janne Keränen), and M.F.F. All authors have read and agreed to the published version of the manuscript.

Funding: This work was fully supported by the EU REFLECTIVE project, funded by the European Union's Horizon 2020 research and innovation program under grant agreement No. 101006747.

Data Availability Statement: Data are available on request due to restrictions.

Acknowledgments: The authors wish to thank Petr Hajduk for generating the driving cycles used in this work.

Conflicts of Interest: All the authors declare that the research was conducted in the absence of any commercial or financial relationships that could be construed as a potential conflict of interest.

References

1. Friedrich, M.; Ge, J.; Vigna, L. 4 Charts Explain Greenhouse Gas Emissions by Countries and Sectors. Available online: <https://www.wri.org/insights/4-charts-explain-greenhouse-gas-emissions-countries-and-sectors#> (accessed on 9 October 2023).
2. Carbon Dioxide Emissions from the Transportation Sector Worldwide from 1970 to 2022. Available online: <https://www.statista.com/statistics/1291615/carbon-dioxide-emissions-transport-sector-worldwide/> (accessed on 1 November 2023).
3. Regulation (EU) 2019/631 of the European Parliament and of the Council of 17 April 2019 Setting CO₂ Emission Performance Standards for New Passenger Cars and for New Light Commercial Vehicles, and Repealing Regulations (EC) No. 443/2009 and (EU) No 510/2011. Available online: <https://eur-lex.europa.eu/legal-content/EN/TXT/?uri=CELEX%3A02019R0631-20210301> (accessed on 1 November 2023).
4. Greene, D.L.; Park, S.; Liu, C. Public Policy and the Transition to Electric Drive Vehicles in the U.S.: The Role of the Zero Emission Vehicles Mandates. *Energy Strategy* **2014**, *5*, 66–77. [CrossRef]
5. Li, C.; Negnevitsky, M.; Wang, X.; Yue, W.L.; Zou, X. Multi-criteria Analysis of Policies for Implementing Clean Energy Vehicles in China. *Energy Policy* **2019**, *129*, 826–840. [CrossRef]
6. Åhman, M. Government Policy and the Development of Electric Vehicles in Japan. *Energy Policy* **2006**, *34*, 433–443. [CrossRef]
7. Allwood, J.M.; Dunant, C.F.; Lupton, R.C.; Cleaver, C.J.; Serrenho, A.C.H.; Azevedo, J.M.C.; Horton, P.M.; Clare, A.; Low, H.; Horrocks, I.; et al. *Absolute Zero: Delivering the UK's Climate Change Commitment with Incremental Changes to Today's Technologies*, 1st ed.; University of Cambridge: Cambridge, UK, 2019.
8. CO₂ Emission Performance Standards for Cars and Vans. Available online: https://climate.ec.europa.eu/eu-action/transport/road-transport-reducing-co2-emissions-vehicles/co2-emission-performance-standards-cars-and-vans_en (accessed on 1 November 2023).
9. Zhou, W.; Cleaver, C.J.; Dunant, C.F.; Allwood, J.M.; Lin, J. Cost, Range Anxiety and Future Electricity Supply: A Review of How Today's Technology Trends May Influence the Future Uptake of BEVs. *Renew. Sustain. Energy Rev.* **2023**, *173*, 113074. [CrossRef]
10. Ehrenberger, S.; Dasgupta, I.; Brost, M.; Gebhardt, L.; Seiffert, R. Potentials of Light Electric Vehicles for Climate Protection by Substituting Passenger Car Trips. *World Electr. Veh. J.* **2022**, *13*, 183. [CrossRef]
11. Regulation (EU) No 168/2013 of the European Parliament and of the Council of 15 January 2013 on the Approval and Market Surveillance of Two- or Three-Wheel Vehicles and Quadricycles (Text with EEA Relevance). Available online: <http://data.europa.eu/eli/reg/2013/168/2020-11-14> (accessed on 9 October 2023).
12. Lindh, P.; Gerami Tehrani, M.; Lindh, T.; Montonen, J.H.; Pyrhönen, J.; Sopanen, J.T.; Niemelä, M.; Alexandrova, Y.; Immonen, P.; Aarniovuori, L.; et al. Multidisciplinary Design of a Permanent-Magnet Traction Motor for a Hybrid Bus Taking the Load Cycle into Account. *IEEE Trans. Ind. Elect.* **2016**, *63*, 3397–3408. [CrossRef]
13. Ruuskanen, V.; Nerg, J.; Parviainen, A.; Rilla, M.; Pyrhönen, J. Design and Drive-cycle Based Analysis of Direct-driven Permanent Magnet Synchronous Machine for a Small Urban Use Electric Vehicle. In Proceedings of the 16th European Conference on Power Electronics and Applications, Lappeenranta, Finland, 26–28 August 2014.
14. Ruuskanen, V.; Nerg, J.; Pyrhönen, J.; Ruotsalainen, S.; Kennel, R. Drive Cycle Analysis of a Permanent-Magnet Traction Motor Based on Magnetostatic Finite-Element Analysis. *IEEE Trans. Veh. Technol.* **2015**, *64*, 1249–1254. [CrossRef]
15. Łebkowski, A. Light Electric Vehicle Powertrain Analysis. *Sci. J. Silesian Univ. Technol. Ser. Transp.* **2017**, *94*, 123–137. [CrossRef]
16. Chirca, M.; Dranca, M.A.; Breban, S.; Oprea, C.A. PMSM Evaluation for Electric Drive Train for L6e Light Electric Vehicles. In Proceedings of the International Conference and Exposition on Electrical and Power Engineering (EPE), Iasi, Romania, 22–23 October 2020.
17. Houache, M.; Yim, C.-H.; Karkar, Z.; Abu-Lebdeh, Y. On the Current and Future Outlook of Battery Chemistries for Electric Vehicles—Mini Review. *Batteries* **2022**, *8*, 70. [CrossRef]
18. Anttila, J.; Todorov, Y.; Ranta, M.; Pihlatie, M. System-Level Validation of an Electric Bus Fleet Simulator. In Proceedings of the IEEE Vehicle Power and Propulsion Conference (VPPC), Hanoi, Vietnam, 14–17 October 2019.
19. Joksimović, G.; Levi, E.; Kajević, A.; Mezzarobba, M.; Tassarolo, A. Optimal Selection of Rotor Bar Number for Minimizing Torque and Current Pulsations Due to Rotor Slot Harmonics in Three-Phase Cage Induction Motors. *IEEE Access* **2020**, *8*, 228572–228585. [CrossRef]
20. Tapani, J.; Hrabovcova, V.; Pyrhonen, J. *Design of Rotating Electrical Machines*, 2nd ed.; John Wiley & Sons: West Sussex, UK, 2013.
21. AC Motor Controller Gen4 Size 8. Available online: https://cdn.borgwarner.com/docs/default-source/default-document-library/gen4-size-8.pdf?sfvrsn=4b2b5a3d_7 (accessed on 9 October 2023).
22. Superior Lithium Ion Battery. Available online: https://www.master-instruments.com.au/files/battery_information/kokam_cell_brochure2021.pdf (accessed on 9 October 2023).
23. Kokam Li-ion Cell, Kokam. 2021. Available online: <https://kokam.com/en/product/cell/lithium-ion-battery> (accessed on 9 October 2023).
24. Needell, Z.A.; Trancik, J.E. Efficiently Simulating Personal Vehicle Energy Consumption in Mesoscopic Transport Models. *Transp. Res. Rec.* **2018**, *2672*, 163–173. [CrossRef]

Disclaimer/Publisher's Note: The statements, opinions and data contained in all publications are solely those of the individual author(s) and contributor(s) and not of MDPI and/or the editor(s). MDPI and/or the editor(s) disclaim responsibility for any injury to people or property resulting from any ideas, methods, instructions or products referred to in the content.